IARJSET

ISSN (Online) 2393-8021
ISSN (Print) 2394-1588

International Advanced Research Journal in Science, Engineering and Technology

Vol. 6, Issue 7, July 2019

Numerical and Spatial Analysis of Jeffrey Nanofluid Explored using CNT Over a Stretched / Shrinking Sheet with Suction and Injection

P.S.S. Nagalakshmi

Assistant Professor in the Department of Digital Technology in JNAFAU, India

Abstract: The aspiration of current study is to address the Magneto Hydro Dymaics (MHD) radiative flow of an incompressible steady flow of Jeffrey nanofluid explored using CNT (single and multi walled carbon nanotubes) over a stretched /shrinking surface. Heat and mass transfer characteristics are accounted for in the presence of joule heating and thermo-phoretic effects along with viscous dissipation. The governing non-linear partial differential equations are reduced to non-linear ordinary differential equations by using some adequate dimensionless variables and then solved numerically with Runge-Kutta method. The optimal solution expression of velocity, temperature, and concentration are explored through spatial representations by using several values of physical constraints with contour plot and surface plots. Further the coefficient of skin friction and local Nusselt number are examined through graphs. Artificial neural network introduced at this juncture to obtain the predictive values of engineering constraints from physical constraints.

Keywords: MHD, CNT, Contour, 3d Surface, ANN

I. INTRODUCTION

The idea of dispersing solids in fluids was first proposed by Maxwell via his theoretical work more than 120 years ago [1]. It was later used to disperse mm and/or µm sized particles in fluids by Ahuja in 1975,Liu et al. in 1988, and researchers at Argonne National Laboratory (ANL) in 1992 [2–6]. Their work depended on the high thermal conductivity of metals at room temperature compared to fluids (i.e., order of magnitude higher in thermal conductivity). One of the problems that arise from using fluids containing µm sized particles is the clogging of small passages caused from the large agglomeration of the solid particles, making it therefore hard to employ in heat transfer equipment fitted with small passages. The experimental study of copper suspended in water to enhance the heat transfer and reduce pumping power in a heat exchanger was carried out by Choi and Eastman (1995) [7]. On the other hand, nanofluids are believed to surpass such obstacle due to containing small enough particle size which can flow smoothly through such channels. Another advantage of using nanoparticles is that they have an extremely large surface area over which the heat transfer mechanism between the particle and its surrounding takes place. For such reason, decreasing the size of particles from mm and µm down to nm would extremely larger the surface area and with it the enhancement in heat transfer. The thermal conductivity of nanofluids has been calculated theoretically, and the results showed a high thermal conductivity compared with the base fluid. Metals have higher thermal conductivities than fluids at room temperature, the thermal conductivity of metallic liquids is much greater than that of non-metallic liquids. Therefore the thermal conductivities of fluids that contain suspended solid metallic particles could be expected to be significantly higher than those of conventional heat transfer fluids. Nanomaterials used in nanofluids to date include metals, non-metals and carbons. These nanomaterials also come in a wide variety of morphologies that include particles, fibers & tubes [8–10]. Carbon is one of the most abundant elements in the Earths biosphere. Nature has used this element, coupled predominantly with oxygen and hydrogen to form a diverse range of organic compounds. Furthermore, carbon atoms can bond with themselves in a number of different ways to form a variety of carbon materials or allotropes of carbon. Each of these allotropes has differences in their respective material properties. Typical carbon allotropes include amorphous carbon, diamond and graphite. Carbon allotropes can also have a variety of structures and morphologies such as crystalline (i.e., diamond, three dimensional, 3D), graphite sheets (2D) and carbon nanotubes (1D). Moreover, the discovery of Buckminster-fullerenes, or Bucky balls by Kroto et al. in the mid-1980s[11], stimulated the search for new forms of carbonaceous materials. Carbon nanomaterials are of particular interest, since they are black in color, which makes them ideal for solar absorption applications. In addition, their very high thermal conductivity also makes them ideal additives for nanofluids [12–14]. For example, the thermal conductivity of carbon nanotubes (2000 to 6000 $Wm^{-1}K^{-1}$) are an order of magnitude higher than metals like Au (315 $Wm^{-1}K^{-1}$) and Cu (398 $Wm^{-1}K^{-1}$), and metal oxides such as Al_2O_3 (40 $Wm^{-1}K^{-1}$) and CuO (77 $Wm^{-1}K^{-1}$). New forms of carbon nanomaterials include:

(1) single and multi-wall carbon nanotubes [15,16]; (2) nanoballs [17]; (3) fullerenes C70, C76 [18], C84 [19], C60 in a crystalline form, nanocones [20], nanohorns [21], nanofilaments [22], nanocapsules [23]; (4) graphite nanoparticles [24]; (5) graphene and graphene oxide [25,26]; (6) carbon black [27,28], and (7) carbon nanospheres (CNS) [29,30]. Sen Gupta et al. [31] carried out an experimental study to measure the thermal conductivity in graphene nanofluids using the transient hot wire method. They also studied carbon nanotube (CNT) and graphene oxide nanofluids. The magnitude of enhancement was between CNT and metallic/metal oxide nanofluids.

There are two main kinds of nanotubes: single-walled carbon nanotubes (SWCNTs),individual cylinders of 1-2 nm in diameter, consisting of a single rolled graphene sheet, andmulti-walled carbon nanotubes (MWCNTs), a ―Russian doll‖ structure constituted by several concentric graphene cylinders, where weak Van der Waals forces bind the tubes together [32].Thus, SWCNTs are significantly smaller in diameter compared to MWCNTs and the thermal properties may differ significantly. Diameter and length are two key parameters to describe CNTs and directly affects thermal conductivity performance of both CNTs and composites containing CNTs. Cao et al. [33] reported the thermal conductivity to be theoretically higher for SWCNTs with smaller diameters. Fujii et al. [34] measured the thermal conductivity of a single MWCNT by using a suspended sample-attached T-type nanosensor. The thermal conductivity of MWCNT at room temperature increased as its diameter decreased, i.e the thermal conductivity increased as the number of walls decreased, varying from about 500 W/m·K for an outer diameter of 28 nm to 2069 W/m·K for diameter 10nm.For length parameters (L) from 5 to 350 nm, the calculated thermal conductivity increased with increasing tube length and followed a L^{α} law, with α values between 0.54 (100 nm < L < 350 nm) and 0.77 (L < 25 nm).

The study of fluid flow over stretching sheet has gained considerable attention due to its occurrence in many industry and manufacturing processes, such as polymer sheet or filament extrusion from a dye or long thread between feed roll or wind-up roll, glass-fibre, paper production, drawing of plastic films, drawing of copper wires, metal extrusion, plastics manufacturing, wire and blade coating, dying of paper and textile, polymer industries, food processing, geophysics and chemical and petroleum processes and etc. The most common and simplest model of non-Newtonian fluids is Jeffrey fluid which has time derivative instead of convected derivative. I. S. Awaludin et al. [35] studied the Stability analysis of stagnation-point flow over a stretching/shrinking sheet. Maria Imtiaz et al. [36] reported the MHD Convective Flow of Jeffrey Fluid Due to a Curved Stretching Surface with Homogeneous-Heterogeneous Reactions. N. Sandeep and C. Sulochana are [37] examined the Momentum and heat transfer behaviour of Jeffrey, Maxwell and Oldroyd-B nanofluids past a stretching surface with non-uniform heat source/sink. Kartini Ahmad et al. [38] studied Mixed convection Jeffrey fluid flow over an exponentially stretching sheet with magneto hydrodynamic effect. Tasawar Hayat et al. [39] discussed the MHD stagnation point flow of Jeffrey fluid by a radially stretching surface with viscous dissipation and Joule heating. Kalidas Das et al. [40] reported the Radiative flow of MHD Jeffrey fluid past a stretching sheet with surface slip and melting heat transfer. Hayat T et al. [41] examined Thermal and Concentration Stratifications Effects in Radiative Flow of Jeffrey Fluid over a Stretching Sheet. Sakiadis [42] was the first to study the boundary layer flow over stretched surface with a constant velocity and formulated a boundary-layer equation for two-dimensional and axisymmetric flows, which is later extended by Crane[43], who investigated the problem of a stretching sheet whose velocity is proportional to the distance from the slit. Since then, lots of studies have been carried out taking into account the effect of stretching along with various physical effects. Qasim [44] investigated the effects of heat and mass transfer in Jeffrey fluid over a stretching sheet in the presence of heat source/sink, Cortell [45] studied the boundary layer flow induced in a quiescent fluid by a continuous sheet stretching, Ahmad and Ishak [46] studied MHD flow and heat transfer of a Jeffrey fluid towards a stretching vertical surface and to name a few.

II. MATHEMATICAL FORMULATION

Consider the Cartesian coordinate system in such a way that x-axis is along the stretched surface and y axis is perpendicular to x-axis. Magneto hydrodynamics boundary layer steady flow of a electrically conducting incompressible Jeffrey nanofluid is considered. A uniform magnetic field B_0 is applied parallel to the y-axis .The induced magnetic field is neglected for small magnetic reynold number. Heat and mass transfer characteristics are taken into account in the presence of thermal radiation and thermophoresis effects. The uniform temperature of the surface T_w is larger than ambient fluid temperature T_∞. The species concentration at the surface C_w and ambient concentration C_∞ are constants. The following governing equations are introduced

$$\frac{\partial u}{\partial x}+\frac{\partial v}{\partial y}=0$$

$$u\frac{\partial u}{\partial x}+v\frac{\partial u}{\partial y}=\frac{v_{nf}}{1+\lambda}\left[\frac{\partial^2 u}{\partial y^2}+\lambda_1\left(u\frac{\partial^3 u}{\partial x\partial^2 y}-\frac{\partial u}{\partial x}\frac{\partial^2 u}{\partial y^2}+\frac{\partial u}{\partial y}\frac{\partial^2 u}{\partial x\partial y}+v\frac{\partial^3 u}{\partial y^3}\right)\right]-\frac{\sigma_{nf}}{\rho_{nf}}{B_0}^2 u$$
$$+g[\beta_T(T-T_\infty)+\beta_C(C-C_\infty)]$$

$$u\frac{\partial T}{\partial x}+v\frac{\partial T}{\partial y}=\frac{k_{nf}}{(\rho c_p)_{nf}}\frac{\partial^2 T}{\partial y^2}+\frac{\mu_{nf}}{(\rho c_p)_{nf}}\left(\frac{\partial u}{\partial y}\right)^2+\frac{\sigma_{nf}}{(\rho c_p)_{nf}}B_0^2u^2+\frac{16\sigma T_\infty^3}{3k^s}\frac{\partial^2 T}{\partial y^2}$$

$$u\frac{\partial C}{\partial x}+v\frac{\partial C}{\partial y}=D\frac{\partial^2 C}{\partial y^2}-k_0(C-C_\infty)-\frac{\partial}{\partial y}\left(V_T(C-C_\infty)\right)$$

Where u and v are the velocity components in x and y directions respectively, x is the distance along the sheet; ν_{nf} kinematic nanofluid viscosity,λ and λ_1 are the ratio of relaxation and retardation time respectively, ρ_{nf} density of nanofluid, σ_{nf} electrical conductivity of nanofluid, g the gravitational acceleration β_T and β_C thermal expansion coefficients temperature, c_p specific heat ,σ the Stefan-Boltzmann constant, k^s the mean absorption coefficient ,D the diffusion coefficient and V_T the thermophoretic velocity defined as

$$V_T=-k_1\frac{\nu}{T_{ref}}\frac{\partial T}{\partial y}$$

Boundary conditions are

$$u=u_{w,}v=-v_w,T=T_w,C=C_w aty=0$$

$$u\to 0,\frac{\partial u}{\partial y}\to 0,T\to T_\infty,C\to C_\infty asy\to\infty$$

Where $u_{w,}$ is the stretching \ shrinking velocity,v_w is the wall mass transfer velocity with $v_w > 0$ for mass suction and $v_w < 0$ for mass injection, T_w temperature at the wall, C_w is the concentration at the wall.

$$u_w=ss,T_w=T_\infty+A\left(\frac{x}{L}\right)^2,C_w=C_\infty+bx,\ ss=ax(stretchingsheetcase),$$

$$ss=-ax(shrinkingsheetcase),$$

Where a, b are the positive constants.

Nanofluid parameters are defined as

$$\nu_{nf}=\frac{\mu_{nf}}{\rho_{nf}}$$

$$\rho_{nf}=(1-\varphi)\rho_f+\varphi\rho_{CNT}$$

$$\mu_{nf}=\frac{\mu_f}{(1-\varphi)^{2.5}}$$

$$(\rho c_p)_{nf}=(1-\varphi)(\rho c_p)_f+\varphi(\rho c_p)_{CNT}$$

$$\frac{k_{nf}}{k_f}=\frac{(k_{CNT}+2k_f)-2\varphi(k_f-k_{CNT})}{(k_{CNT}+2k_f)+(k_f-k_{CNT})},$$

$$\frac{\sigma_{nf}}{\sigma_f}=1+\frac{3(\sigma_{CNT}-\sigma_f)\varphi}{(\sigma_{CNT}+2\sigma_f)-(\sigma_{CNT}-\sigma_f)\varphi}$$

Through the following transformations:

$$\psi=\sqrt{a\nu_f}xf(\eta),\eta=\sqrt{\frac{a}{\nu_f}}y,u=\frac{\partial\psi}{\partial y},v=\frac{-\partial\psi}{\partial x}$$

$$u=axf'(\eta),v=-\sqrt{a\nu_f}f(\eta)$$

 DOI 10.17148/IARJSET.2019.6705

IARJSET

ISSN (Online) 2393-8021
ISSN (Print) 2394-1588

International Advanced Research Journal in Science, Engineering and Technology

Vol. 6, Issue 7, July 2019

$$\theta(\eta) = \frac{T - T_\infty}{T_w - T_\infty}, \phi(\eta) = \frac{C - C_\infty}{C_w - C_\infty}$$

The above governing equations are reduced as follows:

$$f''' - \frac{P_2}{P_1}((f')^2 - ff'') + \beta((f'')^2 - ff'''') + \frac{P_3}{P_1}(1+\lambda)Mf' + \gamma(1+\lambda)(\theta + N\phi) = 0$$

$$\left(1 + \frac{4}{3P_5}R\right)\theta'' + \frac{P_4}{P_5}P_r(\theta' f - 2f'\theta) + \frac{P_1}{P_5}P_r E_c (f'')^2 + \frac{P_3}{P_5}ME_c P_r (f')^2 = 0$$

$$\phi'' + S_c(f\phi' - f'\phi) - \frac{k_0}{a}\phi S_c + a\tau S_c(\phi\theta'' + \theta'\phi') = 0$$

The boundary conditions are described as follows.

For stretching sheet

$$f(0) = S, f'(0) = 1, \theta(0) = 1, \phi(0) = 1 at \eta = 0$$

$$f'(\eta) = 0, f''(\eta) = 0, \theta(\eta) = 0, \phi(\eta) = 0 \text{as } \eta = \infty$$

For shrinking sheet

$$f(0) = S, f'(0) = -1, \theta(0) = 1, \phi(0) = 1 at \eta = 0$$

$$f'(\eta) = 0, f''(\eta) = 0, \theta(\eta) = 0, \phi(\eta) = 0 \text{ as } \eta = \infty$$

where

$S = \frac{v_w}{\sqrt{av}}$, is wall mass transfer parameter with $S>0(v_w > 0)$ for wall mass suction and $S<0$ (i.e. $v_w<0$) for wall mass injection,

$P_1 = \frac{1}{(1-\varphi)^{2.5}}(\varphi nanoparticlevolumefraction)$, $P_2 = \left[(1-\varphi) + \varphi\frac{\rho_{CNT}}{\rho_f}\right]$,

$\beta = a\lambda_1(Deborahnumber)$, $P_3 = 1 + \frac{3(\sigma_{CNT} - \sigma_f)\phi}{(\sigma_{CNT} + 2\sigma_f) - (\sigma_{CNT} - \sigma_f)\phi}$, $M = \frac{\sigma_f}{\rho_f}\frac{B_0^2}{a}(Magneticparameter)$,

$\gamma = \frac{Gr_x}{{R_x}^2}(localbuoyancyparameter)$, $Gr_x = g\beta_T(T_w - T_\infty)\frac{\frac{(x^3/v^2)}{u_w^2 x^2}}{v^2}$ (local Grashof number), $R_x = \frac{U_w}{v_f}$, $N = \frac{\beta_c(C_w - C_\infty)}{\beta_T(T_w - T_\infty)}$,

$P_4 = \left[(1-\varphi) + \varphi\frac{(\rho c_p)_{CNT}}{(\rho c_p)_f}\right]$,

$P_5 = \frac{(k_{CNT} + 2k_f) - 2\phi(k_f - k_{CNT})}{(k_{CNT} + 2k_f) + (k_f - k_{CNT})}$, $P_r = \frac{\mu_f (c_p)_f}{k_f}(Prandtlnumber)$, $E_c = \frac{u_w^2}{(c_p)_f(T_w - T_\infty)}(Eckertnumber)$,

$R = \frac{4\sigma T_\infty^3}{k^s k_f}(radiationparameter)$, $\tau = \frac{k_1(T_w - T_\infty)}{T_{ref}}(Thermophoreticparameter)$,

$S_c = \frac{v}{D}(schmidtnumber)$.

DOI 10.17148/IARJSET.2019.6705

Engineering parameters like skin-friction coefficient C_f and local Nusselt number Nu_x, are defined as

$C_f = \frac{\tau_w}{\rho_f u_w^2}$, $Nu_x = \frac{x q_w}{k_f (T_w - T_\infty)}$, where $\tau_w = \mu_{nf} \frac{\partial u}{\partial y}$, is the wall shear-stress and $q_w = -k_{nf} \frac{\partial T}{\partial y}$ is the heat flux at wall.

Using similarity transformation above parameters can be reduced as:

$C_f = (R_x)^{-0.5} (1-\varphi)^{-2.5} f''(0)$, $Nu_x = -(R_x)^{0.5} \frac{k_{nf}}{k_f} \theta'(0)$, Sherwood number

$Sh = -(R_x)^{0.5} \phi^{'(0)}, \text{where} R_x = \frac{U_w}{\nu_f}$.

Thermophysical characteristics of base fluids and CNTs Physical characteristics:

Physical characteristics	Base fluids			Nanoparticles	
	water	Kerosene oil	Engine oil	SWCNTs	MWCNTs
ρ	997.1	783	884	2600	1600
c_p	4179	2090	1910	425	796
k	0.613	0.145	0.144	6600	3000

Numerical Techniques**:**

Coupled ordinary differential equations with boundary conditions are solved numerically using R language with bvp and desolver packages. For the purpose of this shooting iteration techniques together with fourth order Runge Kutta method is considered to determine the velocity, temperature and concentration as the function of coordinate η.There are four asymptotic boundary conditions and hence four unknown surface conditions$f^{'}{}'(0), f^{'''}(0), \theta^{'}(0), \emptyset^{'}(0)$.

III. RESULTS AND DISCUSSION

The objective of the present paper is to study the MHD boundary layer flow of Jeffrey fluid over a stretching/shrinking sheet. The numerical computation is performed for different values of dimensionless parameter involved in the governing equations such as the physical and engineering concern parameter like Magnetic parameter (M),radiation(R r),suction/injection parameter (S),etc. To illustrate the computed results, some figures are plotted and physical explanations are given.

Stretching sheet case:

The variation in velocity $f'(\eta)$ for different value of magnetic parameter M with mass suction/injection are shown in figure 1 and figure 2. We observe that the velocity is decreases with increasing M. Reduction is caused by the Lorentz force, a mechanical force arising due to the interaction of magnetic and electric fields for the motion of an electrically conduction fluid. The Lorentz force increases when M increases and consequently boundary layer thickness in decreases.

The variation in velocity $f'(\eta)$for different values ratio of relaxation/retardation time(λ) is shown in figure 3. We observed that the velocity is increases with increasing (λ) and consequently the thickness of the boundary layer increases.

The variation in velocity $f'(\eta)$for different values ratio of relaxation/retardation time(λ) is shown in figure 4. We observed that the velocity is decreases with increasing (λ) and consequently the thickness of the boundary layer decreases.

The variation in velocity $f'(\eta)$ for different value of magnetic parameter β with mass suction/injection are shown in figure 5 and figure 6. We observe that the velocity is increases with increasing β consequently the thickness of the boundary layer increases.

IARJSET

ISSN (Online) 2393-8021
ISSN (Print) 2394-1588

International Advanced Research Journal in Science, Engineering and Technology

Vol. 6, Issue 7, July 2019

The variation in velocity $\theta(\eta)$for different values of prandtl number (pr) with mass suction is shown in figure 7. We observed that the temperature is increases with increasing pr.

The variation in velocity $\phi(\eta)$for different values of $schmidtnumber$(Sc or S_c or sc) with mass suction is shown in figure 8. We observed that the concentration is decreases with increasing sc.

The variation in velocity $\phi(\eta)$for different values of $schmidtnumber$(Sc or S_c or sc) with mass injection is shown in figure 9. We observed that the concentration is decreases with increasing sc.

The variation in velocity $\phi(\eta)$for different values of thermophoretic parameter (τ) with mass suction is shown in figure 10. We observed that the concentration is increases with increasing τ.

The variation in velocity $\phi(\eta)$for different values of thermophoretic parameter (τ) with mass injection is shown in figure 11. We observed that the concentration is increases with increasing τ.

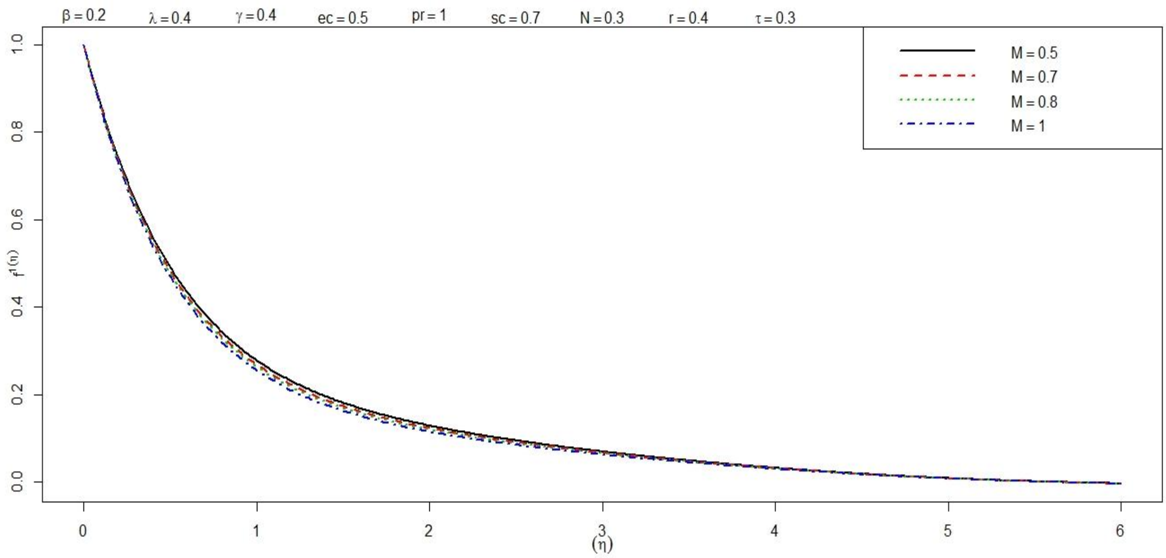

Figure 1: Velocity profiles for different values of Magnetic parameter M with suction

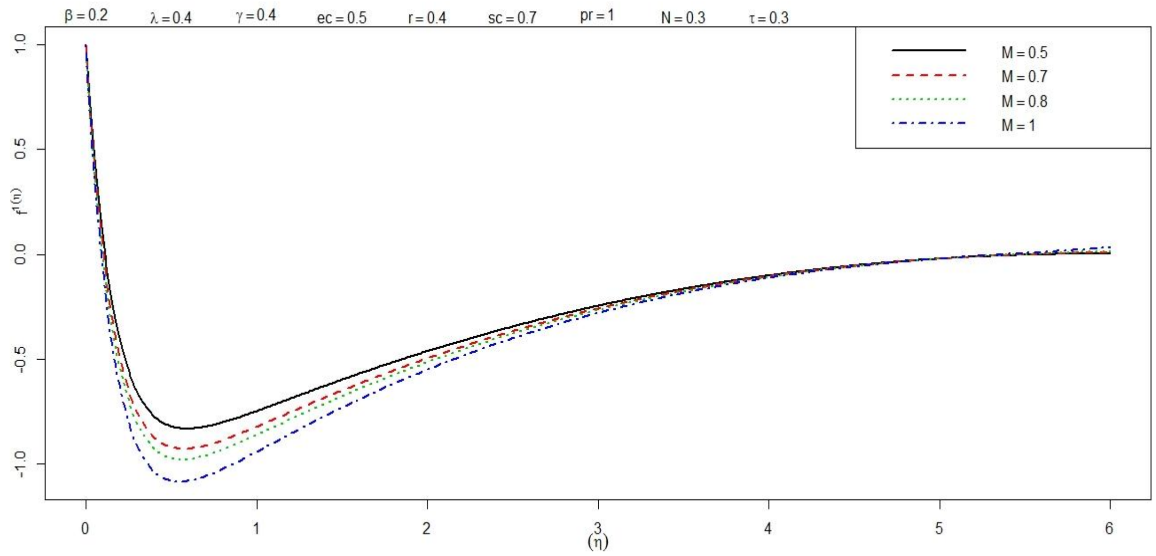

Figure 2: Velocity profiles for different values of Magnetic parameter M with injection

IARJSET

ISSN (Online) 2393-8021
ISSN (Print) 2394-1588

International Advanced Research Journal in Science, Engineering and Technology

Vol. 6, Issue 7, July 2019

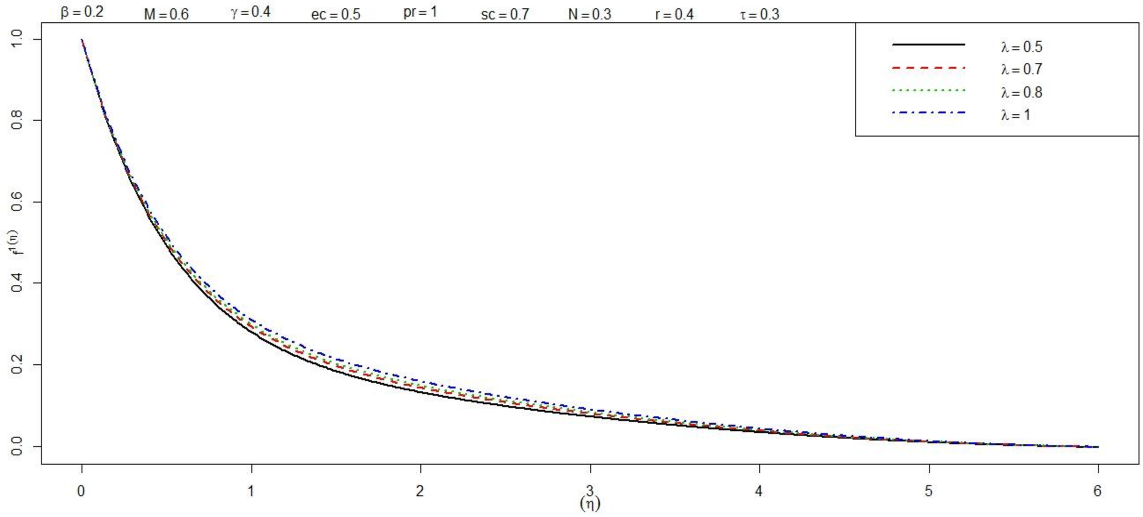

Figure 3: Velocity profiles for different values of ratio of relaxation/retardation time$(\lambda)$with suction

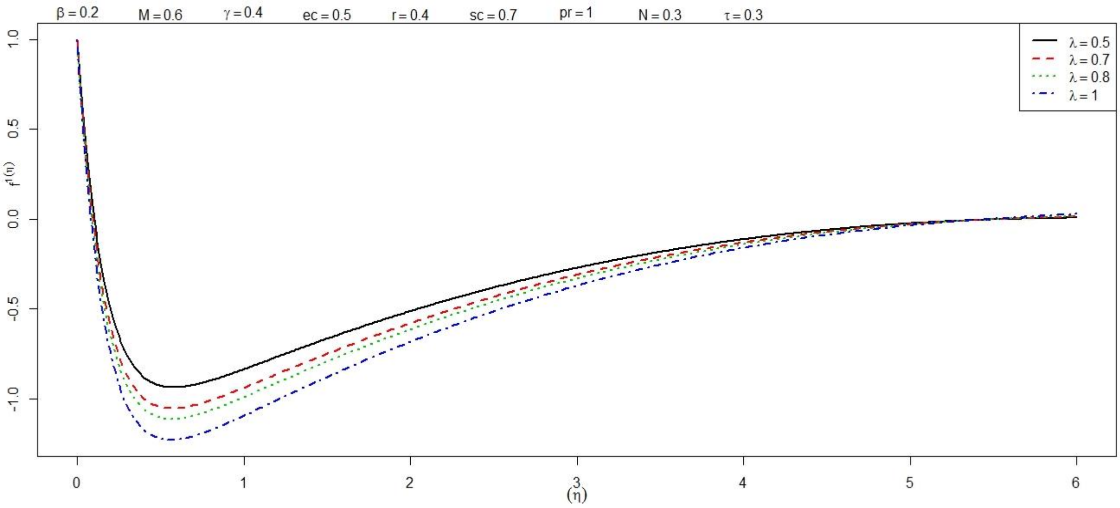

Figure 4: Velocity profiles for different values of ratio of relaxation/retardation time (λ) with injection

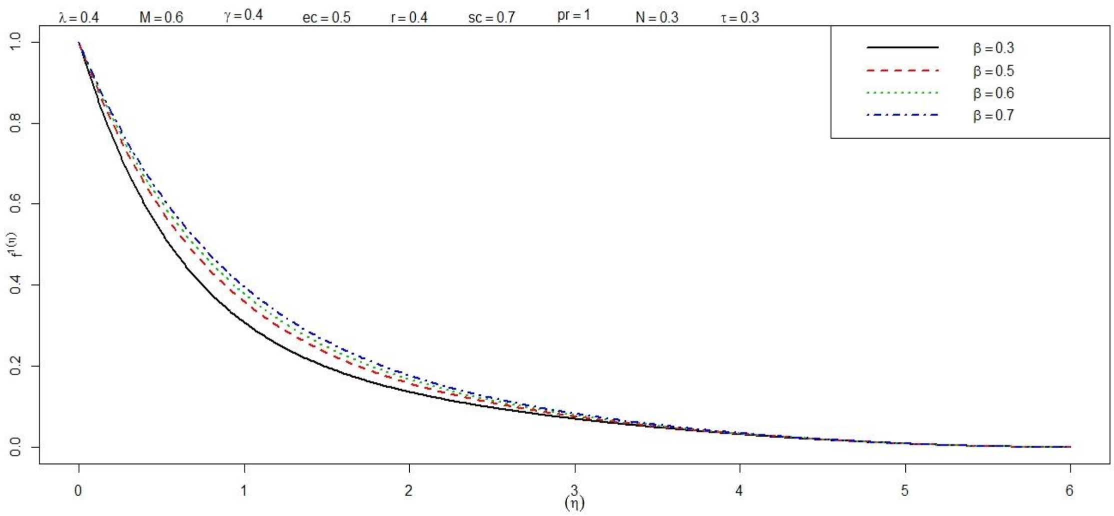

Figure 5: Velocity profiles for different values of Deborah number (β) with suction

IARJSET

ISSN (Online) 2393-8021
ISSN (Print) 2394-1588

International Advanced Research Journal in Science, Engineering and Technology

Vol. 6, Issue 7, July 2019

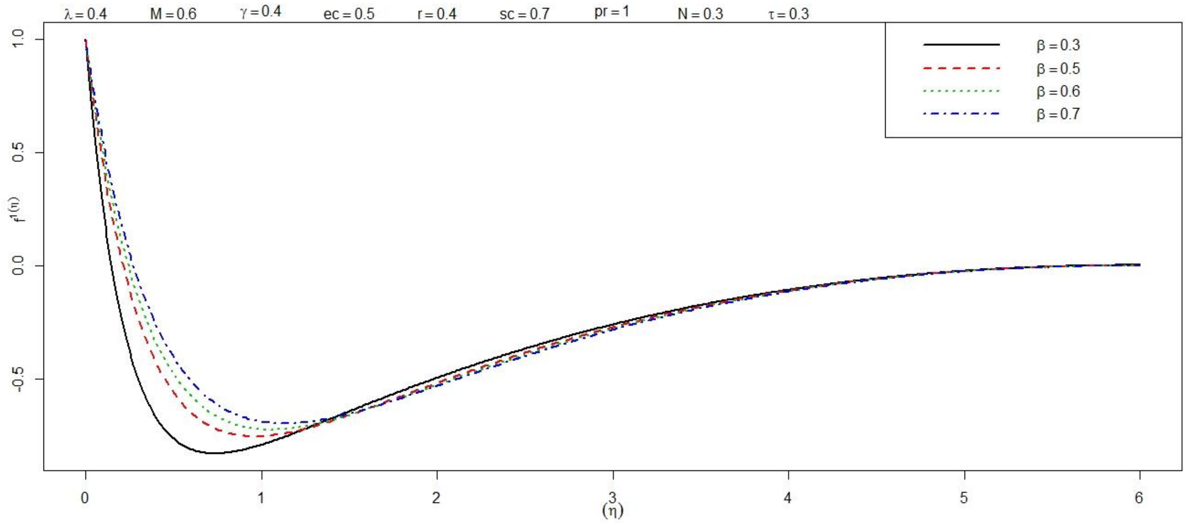

Figure 6: Velocity profiles for different values of Deborah number (β) with injection

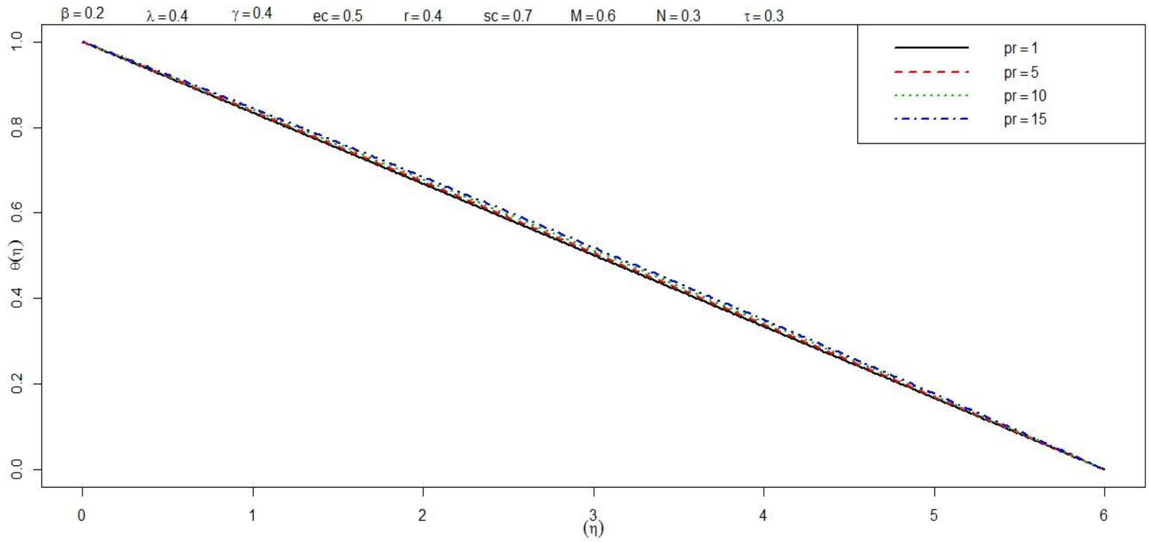

Figure 7: Temperature profile for different values of prandtl number (pr) with suction

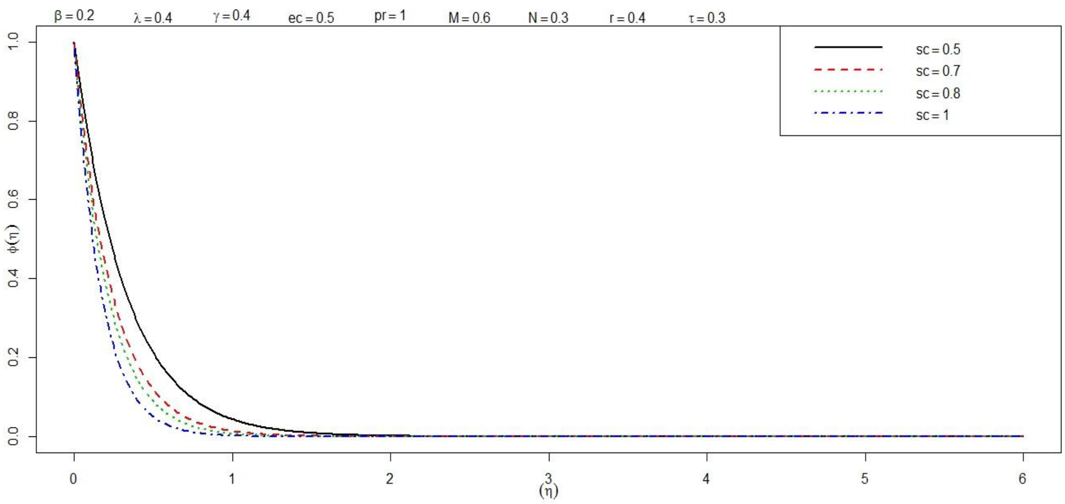

Figure 8: Concentration profile for different values of Schmidt number (sc) with suction

 DOI 10.17148/IARJSET.2019.6705

IARJSET
ISSN (Online) 2393-8021
ISSN (Print) 2394-1588
International Advanced Research Journal in Science, Engineering and Technology
Vol. 6, Issue 7, July 2019

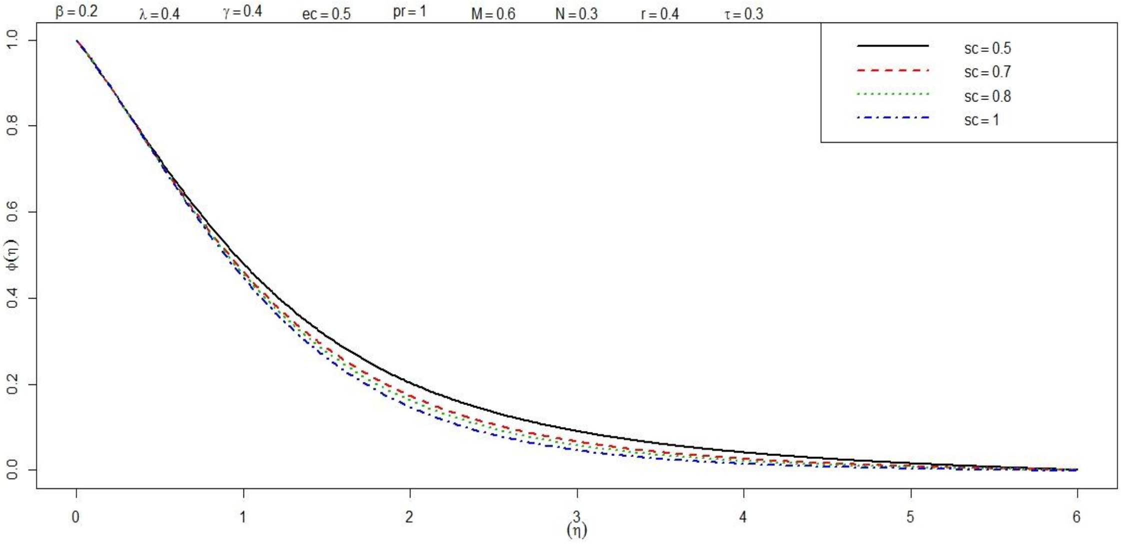

Figure 9: Concentration profile for different values of Schmidt number (sc) with injection

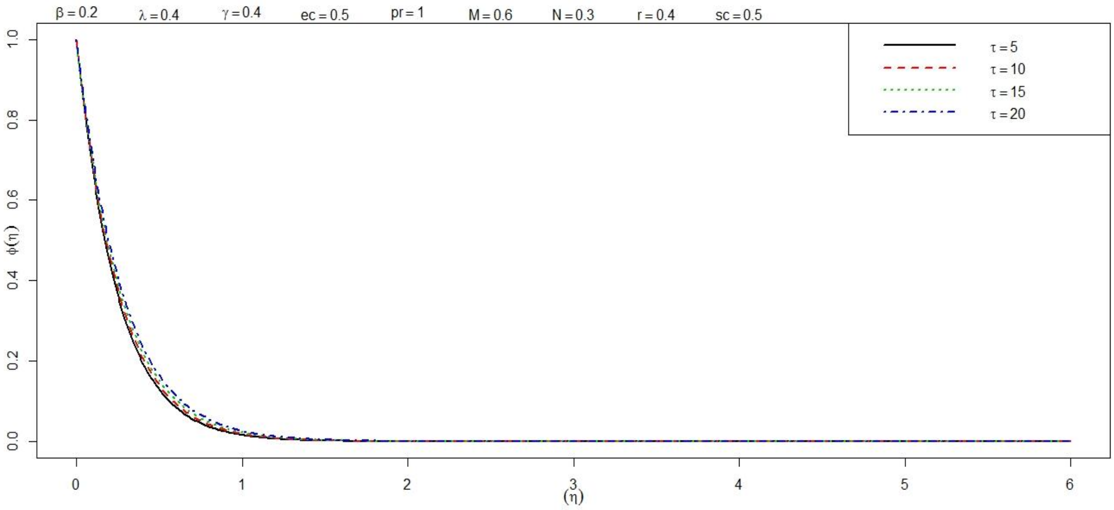

Figure 10: Concentration profile for different values of thermophoretic parameter (τ) with suction

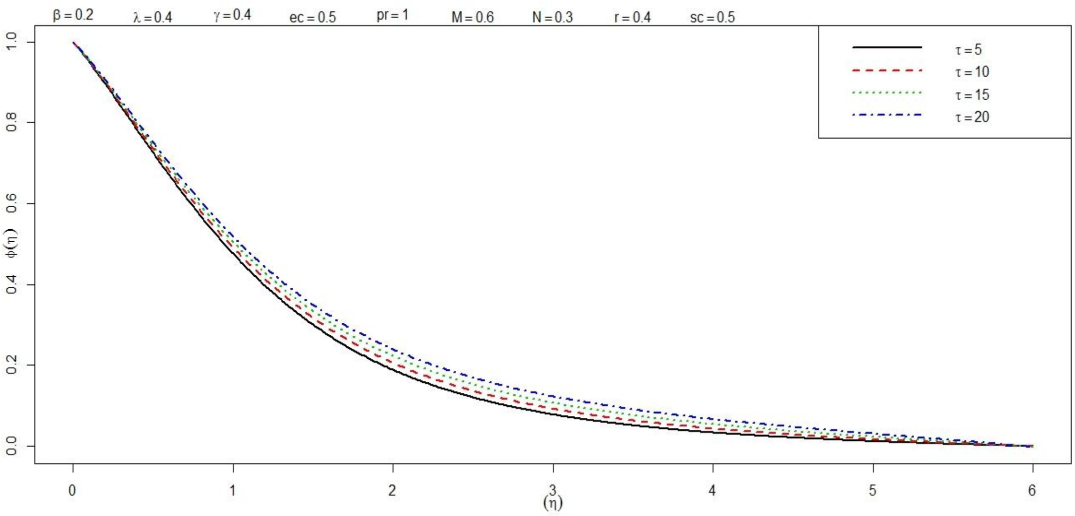

Figure 11: Concentration profile for different values of thermophoretic parameter (τ) with injection

IARJSET

ISSN (Online) 2393-8021
ISSN (Print) 2394-1588

International Advanced Research Journal in Science, Engineering and Technology

Vol. 6, Issue 7, July 2019

Shrinking sheet case

The variation in velocity $f'(\eta)$ for different value of magnetic parameter M with mass suction/injection are shown in figure 12 and figure 13. We observe that the velocity is decreases with increasing M consequently the thickness of the boundary layer increases.

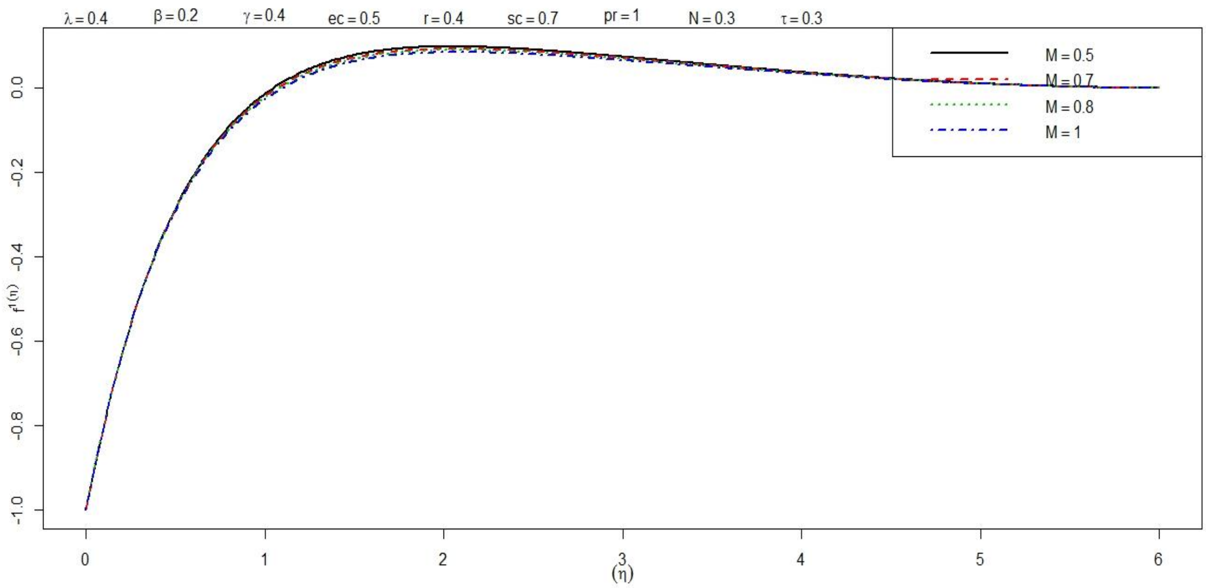

Figure 12: Velocity profiles for different values of Magnetic parameter M with suction

The variation in velocity $f'(\eta)$for different values ratio of relaxation/retardation time(λ) with mass suction /injection are shown in figure 14 and figure 15. We observed that the velocity is increases with increasing (λ) and consequently the thickness of the boundary layer decreases.

The variation in velocity $f'(\eta)$ for different value of magnetic parameter β with mass suction/injection are shown in figure 16 and figure 17. We observe that the velocity is decreases with increasing β consequently the thickness of the boundary layer increases.

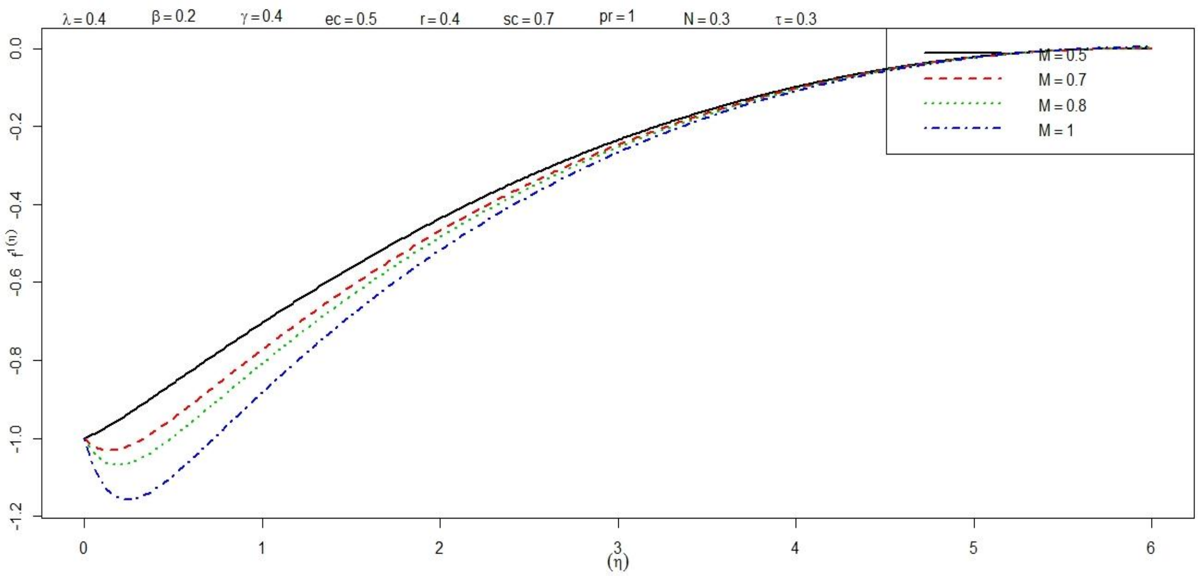

Figure 13: Velocity profiles for different values of Magnetic parameter M with injection

IARJSET

ISSN (Online) 2393-8021
ISSN (Print) 2394-1588

International Advanced Research Journal in Science, Engineering and Technology

Vol. 6, Issue 7, July 2019

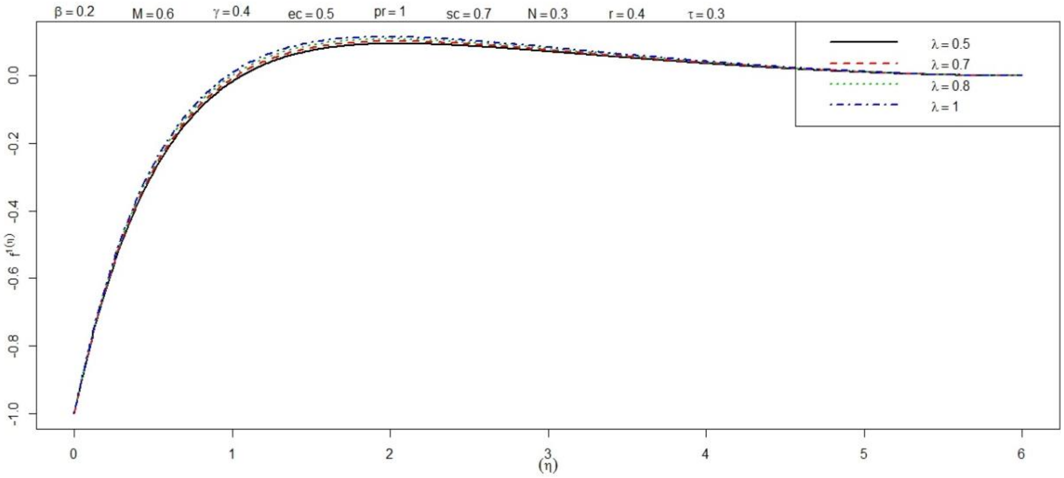

Figure 14: Velocity profiles for different values of ratio of relaxation/retardation time$(\lambda_1)$with suction

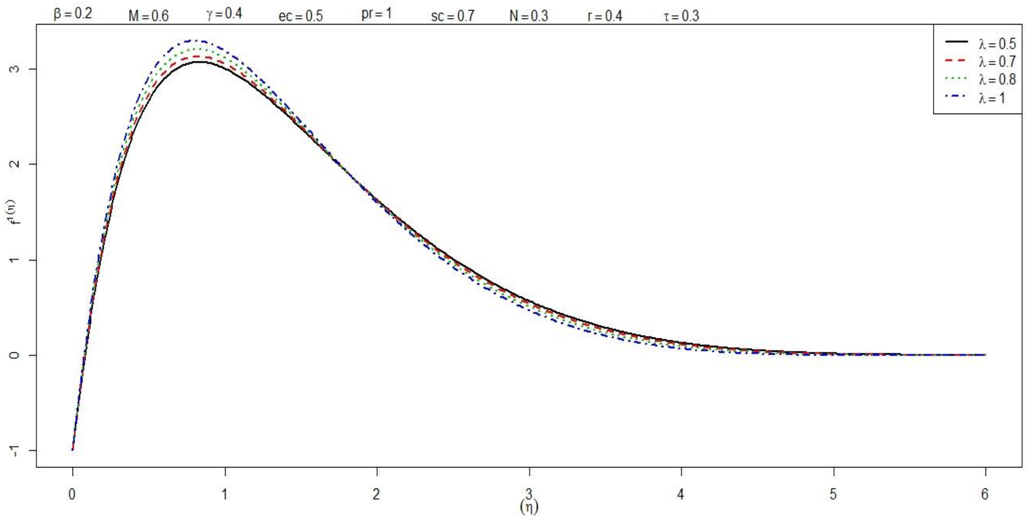

Figure 15: Velocity profiles for different values of ratio of relaxation/retardation time$(\lambda_1)$with injection.

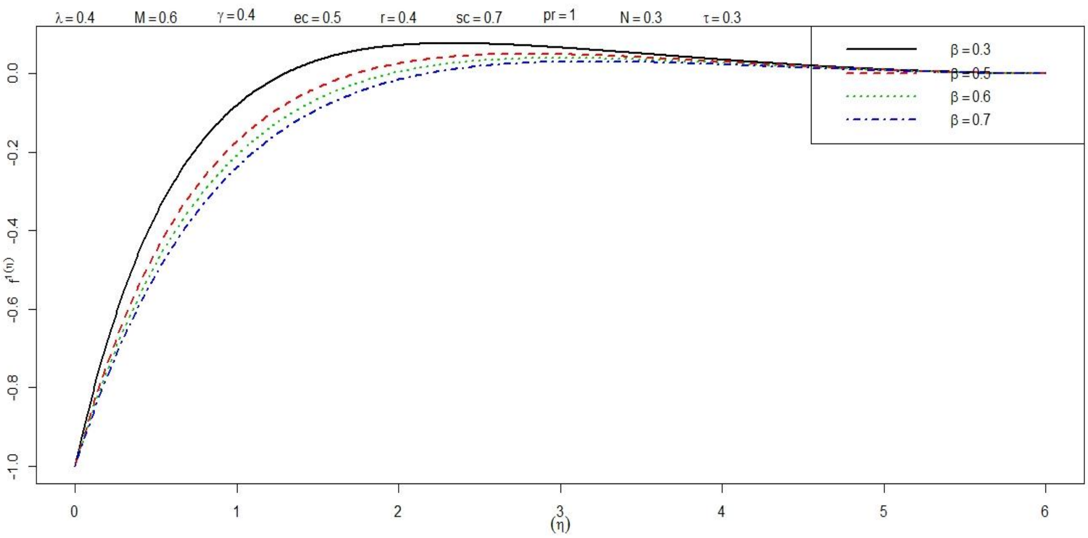

Figure 16: Velocity profiles for different values of Deborah number (β) with suction

IARJSET

ISSN (Online) 2393-8021
ISSN (Print) 2394-1588

International Advanced Research Journal in Science, Engineering and Technology

Vol. 6, Issue 7, July 2019

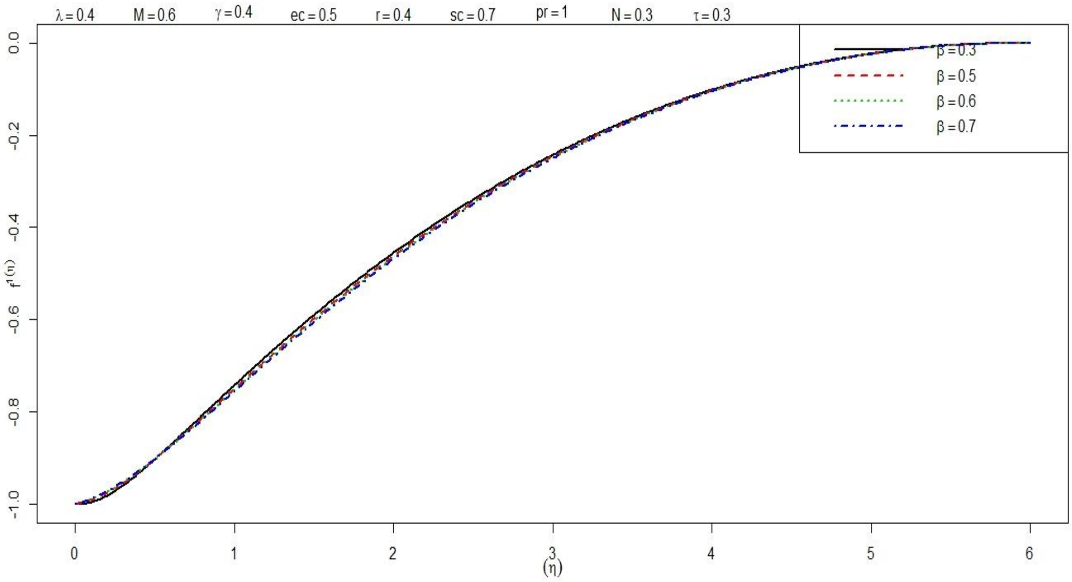

Figure 17: Velocity profiles for different values of Deborah number (β) with injection

Spatial Representation:

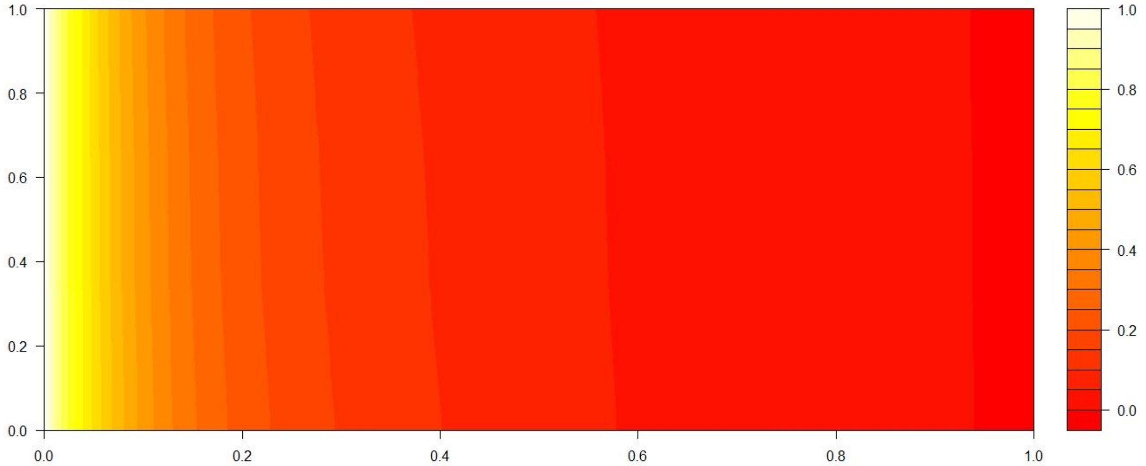

Figure 18: Velocity variations of stretched sheet with wall mass suction using magnetic parameter

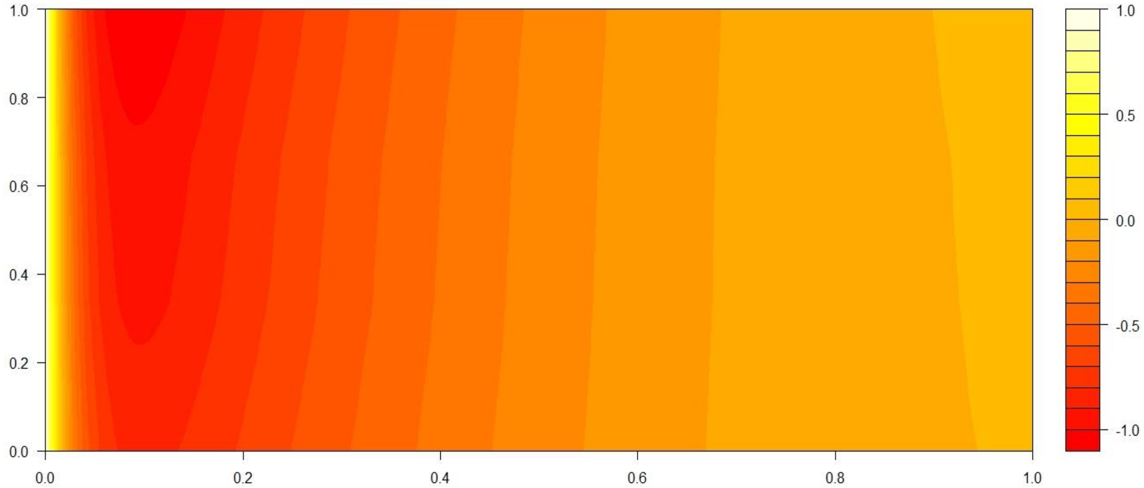

Figure 19: Velocity variations of stretched sheet with wall mass injection using magnetic parameter

ISSN (Online) 2393-8021
ISSN (Print) 2394-1588

International Advanced Research Journal in Science, Engineering and Technology

Vol. 6, Issue 7, July 2019

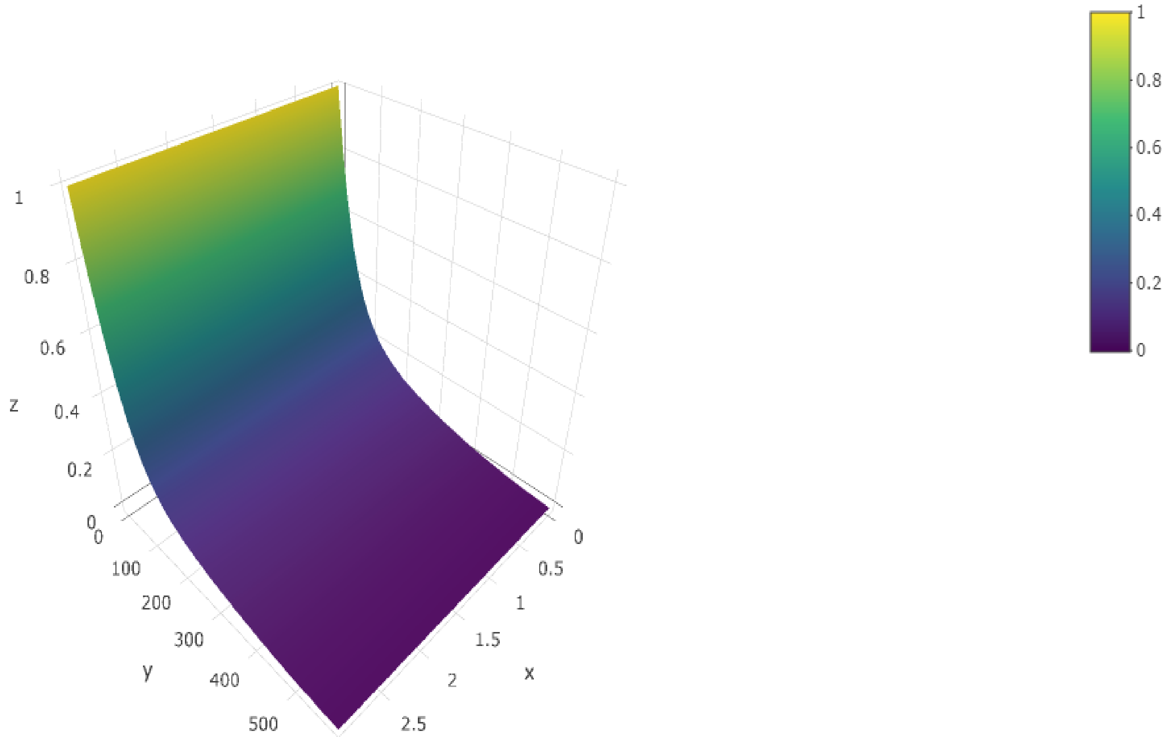

Figure 20: 3D View of Velocity variations of stretched sheet with wall mass suction using magnetic parameter.

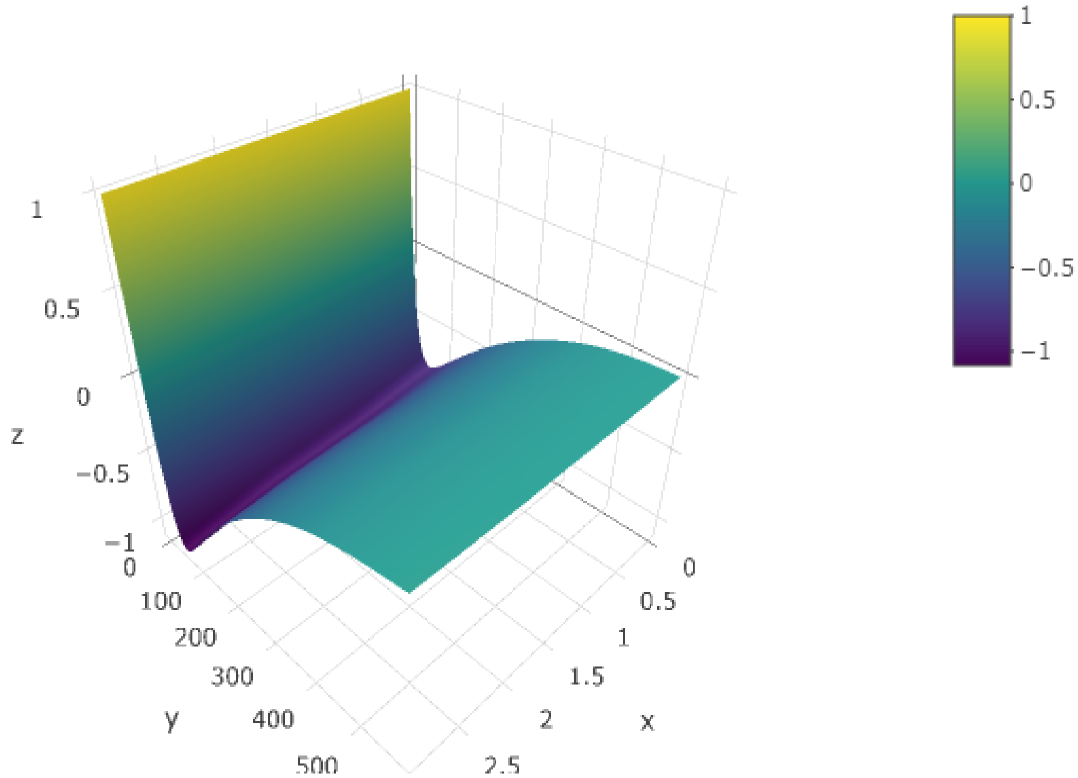

Figure 21: 3D View of Velocity variations of stretched sheet with wall mass injection using magnetic parameter.

IARJSET

ISSN (Online) 2393-8021
ISSN (Print) 2394-1588

International Advanced Research Journal in Science, Engineering and Technology

Vol. 6, Issue 7, July 2019

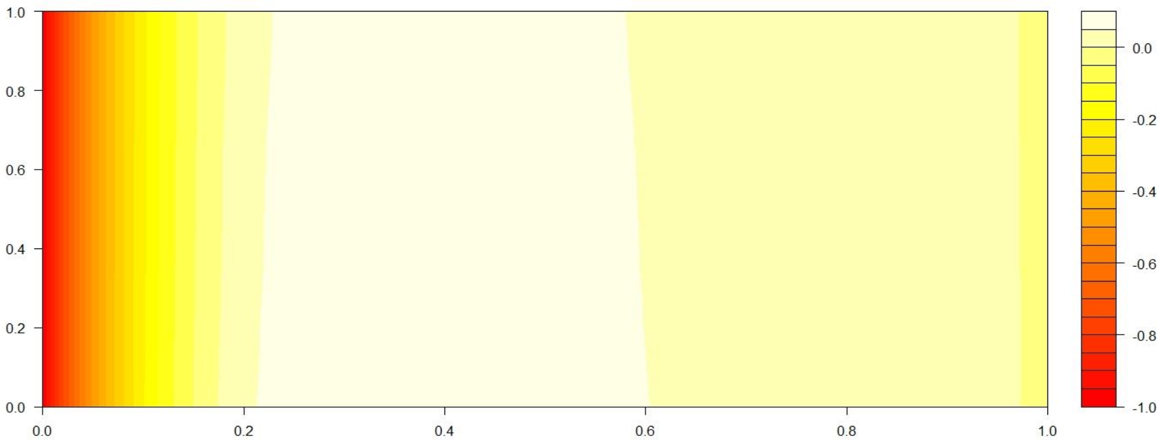

Figure 22: Velocity variations of shrinking sheet with wall mass suction using magnetic parameter.

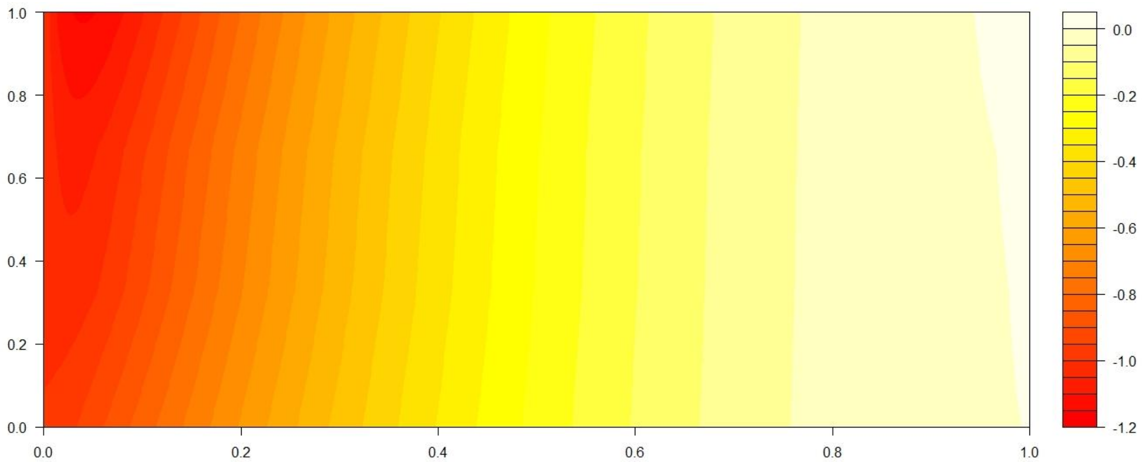

Figure 23: Velocity variations of shrinking sheet with wall mass injection using magnetic parameter.

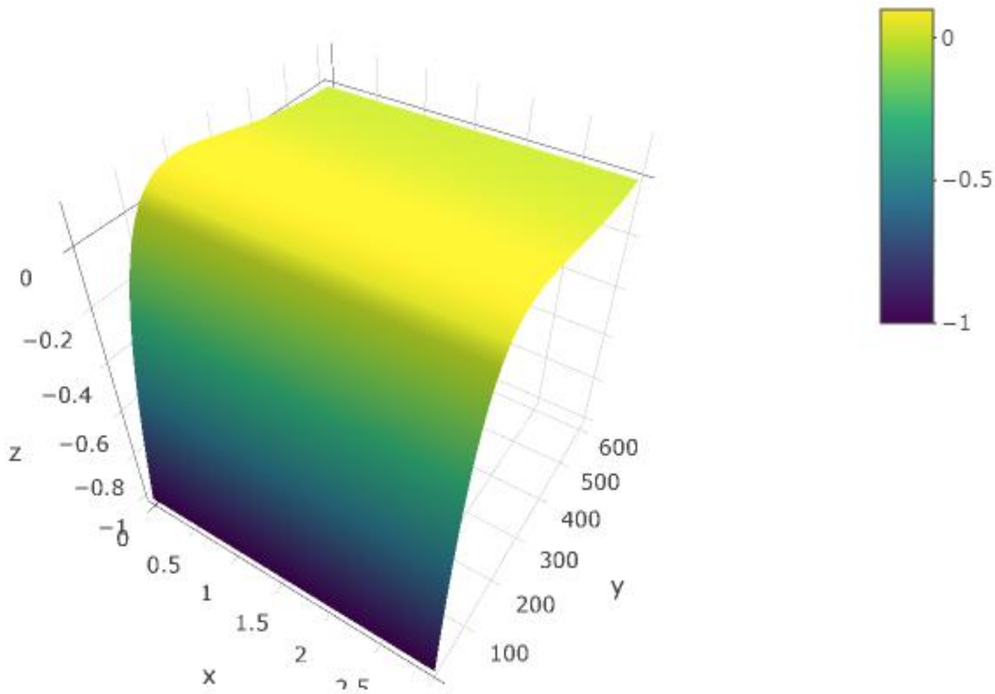

Figure 24: 3D View of Velocity variations of shrinking sheet with wall mass suction using magnetic parameter.

IARJSET

ISSN (Online) 2393-8021
ISSN (Print) 2394-1588

International Advanced Research Journal in Science, Engineering and Technology

Vol. 6, Issue 7, July 2019

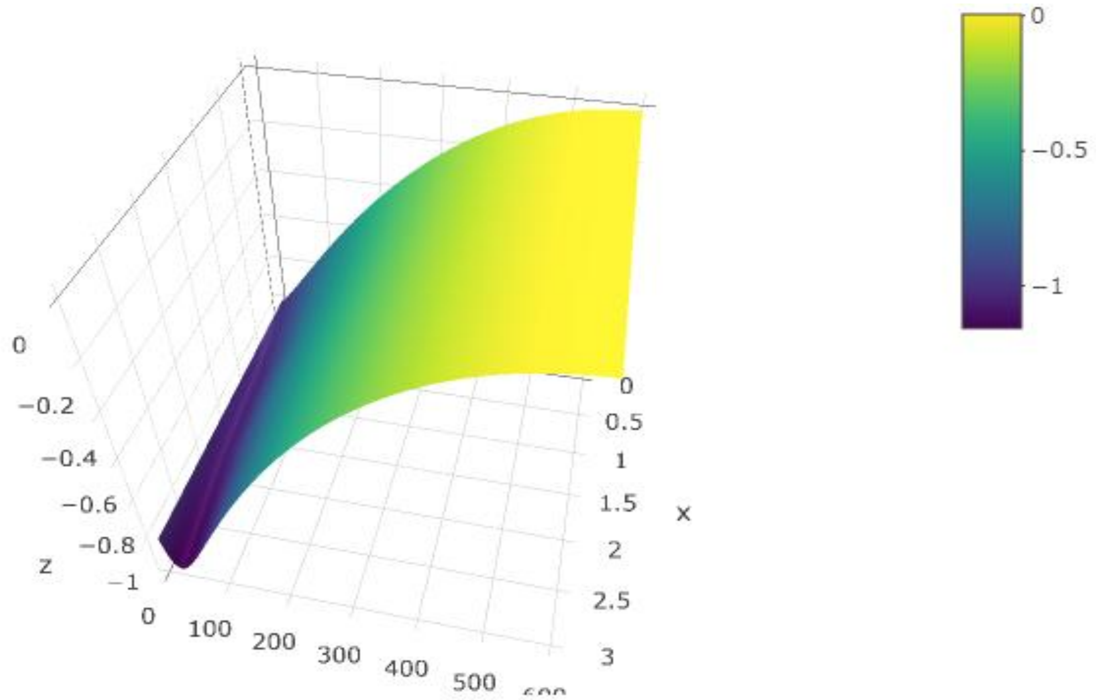

Figure 25: 3D View of Velocity variations of shrinking sheet with wall mass injection using magnetic parameter.

Table 1: Impact of some flow modifying quantities on friction factors, Nusselt and Shearwood number for stretched sheet with suction

M	λ	γ	Ec(ec)	Sc(sc)	$f''(0)$	$-\theta'(0)$	$-\phi'(0)$
0.5					-1.546449019	0.1657288956	4.194738963
0.6					-1.565777615	0.1657381469	4.193997082
0.7					-1.584578136	0.1657471318	4.193277282
0.8					-1.602876090	0.1657558642	4.192578530
	0.5				-1.628637266	0.1657675039	4.191722565
	0.6				-1.619719156	0.1657626138	4.192180963
	0.7				-1.611274713	0.1657579384	4.192616942
	0.8				-1.603276106	0.1657534648	4.193031834
		0.5			-1.561810605	0.1657441364	4.194562653
		0.6			-1.486533862	0.1657167465	4.197819221
		0.7			-1.412180464	0.1656903999	4.201013484
		0.8			-1.338705974	0.1656650479	4.204148624
			0.5		-1.638059154	0.1657726227	4.191240307
			0.6		-1.638061764	0.1658003308	4.191238508
			0.7		-1.638064374	0.1658280391	4.191236710

IARJSET
ISSN (Online) 2393-8021
ISSN (Print) 2394-1588
International Advanced Research Journal in Science, Engineering and Technology
Vol. 6, Issue 7, July 2019

			0.8		-1.638066985	0.1658557474	4.191234911
				0.5	-1.635217502	0.1657722184	3.066314607
				0.6	-1.636893567	0.1657724699	3.630176607
				0.7	-1.638059154	0.1657726227	4.191240307
				0.8	-1.638905800	0.1657727213	4.750235412
β	Pr (pr)	N	R(r)	τ	$f''(0)$	$-\theta'(0)$	$-\phi'(0)$
0.5					-1.1685395322	0.1656908897	4.207652364
0.6					-1.0907339298	0.1656738519	4.210654392
0.7					-1.0287976710	0.1656592996	4.213106507
0.8					-0.9779173695	0.1656466130	4.215163237
	0.5				-1.638286235	0.1662194512	4.191202865
	0.6				-1.638240822	0.1661300545	4.191210355
	0.7				-1.638195408	0.1660406734	4.191217844
	0.8				-1.638149992	0.1659513076	4.191225333
		0.5			-1.634871525	0.1657723699	4.191315231
		0.6			-1.633277846	0.1657722436	4.191352687
		0.7			-1.631684257	0.1657721174	4.191390138
		0.8			-1.630090760	0.1657719912	4.191427585
			0.5		-1.638059169	0.1657726528	4.191240304
			0.6		-1.638059185	0.1657726830	4.191240302
			0.7		-1.638059200	0.1657727131	4.191240299
			0.8		-1.638059215	0.1657727433	4.191240297
				0.5	-1.638047867	0.1657726213	4.184724933
				0.6	-1.638042209	0.1657726206	4.181467662
				0.7	-1.638036541	0.1657726199	4.178210668
				0.8	-1.638030863	0.1657726192	4.174953952

Table 2: Impact of some flow modifying quantities on friction factors, Nusselt and Shearwood number for shrinking sheet with suction

M	λ	γ	Ec(ec)	Sc(sc)	$f''(0)$	$-\theta'(0)$	$-\phi'(0)$
0.5					2.217851270	0.1657288956	3.737104048
0.6					2.217083814	0.1663397027	3.736849911
0.7					2.216828351	0.1663437118	3.736627683
0.8					2.217044017	0.1663476408	3.736434965
	0.5				2.246423258	0.1663516231	3.737625548
	0.6				2.273188673	0.1663481773	3.739062447
	0.7				2.299097107	0.1663449210	3.740444123
	0.8				2.324202629	0.1663418402	3.741774254
		0.5			2.313329227	0.1663395079	3.741709199
		0.6			2.406228909	0.1663249866	3.747126102
		0.7			2.497550707	0.1663116322	3.752391776
		0.8			2.587393084	0.1662993747	3.757516617
			0.5		2.218741421	0.1663552745	3.736129362
			0.6		2.218737695	0.1663948595	3.736126624
			0.7		2.218733968	0.1664344443	3.736123886
			0.8		2.218730242	0.1664740289	3.736121148
				0.5	2.222813864	0.1663551092	2.672517467
				0.6	2.220404137	0.1663552164	3.202705220
				0.7	2.218741421	0.1663552745	3.736129362
				0.8	2.217545112	0.1663553080	4.272053569
β	Pr (pr)	N	R(r)	τ	$f''(0)$	$-\theta'(0)$	$-\phi'(0)$
0.5					1.522408507	0.1664176133	3.700710787
0.6					1.407269005	0.1664365154	3.693838854
0.7					1.315738624	0.1664540518	3.688122339
0.8					1.240676249	0.1664703105	3.683254257
	0.5				2.218526528	0.1665108071	3.736105431

IARJSET

ISSN (Online) 2393-8021
ISSN (Print) 2394-1588

International Advanced Research Journal in Science, Engineering and Technology

Vol. 6, Issue 7, July 2019

	0.6				2.218569506	0.1664796745	3.736110219
	0.7				2.218612485	0.1664485548	3.736115006
	0.8				2.218655463	0.1664174483	3.736119792
		0.5			2.222987259	0.1663552106	3.736272255
		0.6			2.225109778	0.1663551788	3.736343674
		0.7			2.227232031	0.1663551472	3.736415075
		0.8			2.229354018	0.1663551157	3.736486458
			0.5		2.218741406	0.1663552850	3.736129361
			0.6		2.218741392	0.1663552955	3.736129359
			0.7		2.218741377	0.1663553059	3.736129358
			0.8		2.218741363	0.1663553164	3.736129356
				0.5	2.218759811	0.1663552739	3.729129082
				0.6	2.218769036	0.1663552736	3.725629083
				0.7	2.218778280	0.1663552733	3.722129178
				0.8	2.218787544	0.1663552730	3.718629369

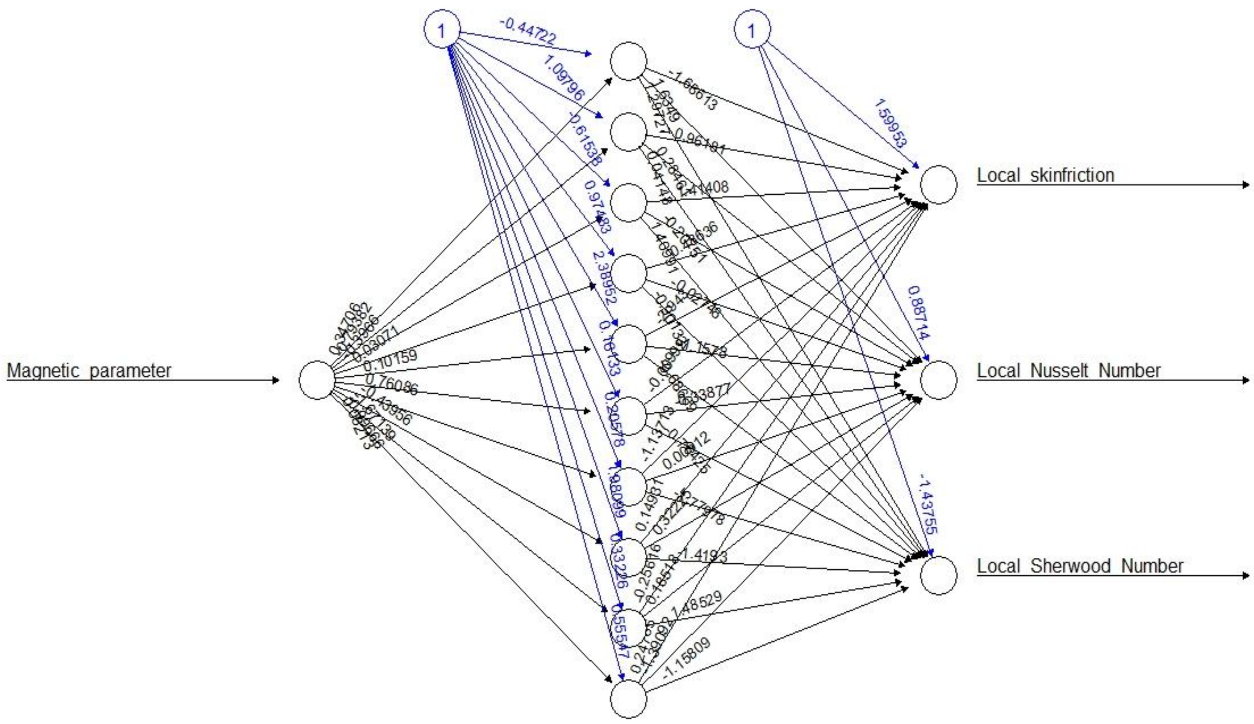

Figure 26: Artificial Neuralnet

Table 3: Impact of magnetic parameter on local friction factors, local Nusselt and local shear wood number for stretched sheet with respect to Runge-Kutta method and Artificial Neural Network.

M	$f''(0)$ R-K Method	$f''(0)$ Neuralnet	$-\theta'(0)$ R-K Method	$-\theta'(0)$ Neuralnet	$-\phi'(0)$ R-K Method	$-\phi'(0)$ Neuralnet
0.5	-1.546449	-1.528794605	0.1657289	0.1423241725	4.194739	4.214508762
0.6	-1.565778	-1.560333307	0.1657381	0.1560706860	4.193997	4.204330328
0.7	-1.584578	-1.592609471	0.1657471	0.1705108718	4.193277	4.189613151
0.8	-1.602876	-1.625574673	0.1657559	0.1855354238	4.192579	4.170506146

REFERENCES

[1]. J.C. Maxwell, A Treatise on Electricity and Magnetism, Claren- don Press, Oxford, UK, 1891.
[2]. S.U.S.Choi, Y. I.Cho, and K.E.Kasza, "Degradation effects of dilute polymer solutionson turbulent friction and heat transfer behavior," Journal of Non-Newtonian Fluid Mechanics, vol. 41, no. 3,pp.289–307, 1992.
[3]. U.Choi,D.M.France, and B.D.Knodel, "Impact of advanced fluids on costs of district cooling systems," in Argonne National Lab, 1992.
[4]. U. Choi and T. Tran, "Experimental studies of the effects of non-Newtonian surfactant solutions on the performance of a shell-and-tube heat exchanger," in Recent Developments in Non- Newtonian Flows and Industrial Applications, The American Society of Mechanical Engineers, NewYork, NY,USA, 1991.
[5]. K.Liu, U.Choi, and K.E.Kasza, Measurements of Pressure Drop and Heat Transfer in Turbulent Pipe Flows of Particulate Slurries, Argonne National Lab., 1988.
[6]. Y.Xuan and Q.Li, "Heat transfer enhancement of nanofluids," International Journal of Heat and Fluid Flow, vol. 21, no. 1, pp. 58–64, 2000.
[7]. Choi, S. U. and Eastman, J. 1995. Enhancing thermal conductivity of fluids with nanoparticles. Developments and Applications of Non-Newtonian Flows, FED 231/MD 66, ASME: 99-105.
[8]. Godson, L.; Raja, B.; Mohan Lal, D.; Wongwises, S. Experimental investigation on the thermal conductivity and viscosity of silver-deionized water nanofluid. Exp. Heat Transf. 2010, 23, 317–332.
[9]. Sani, E.; Mercatelli, L.; Barison, S.; Pagura, C.; Agresti, F.; Colla, L.; Sansoni. P. Potential of carbon nanohorn-based suspensions for solar thermal collectors. Sol. Energy Mater. Sol. Cells 2011, 95, 2994–3000.
[10]. Wen, D.; Ding, Y. Effective thermal conductivity of aqueous suspensions of carbon nanotubes (carbon nanotube nanofluids). J. Thermophys. Heat Transf. 2004, 18, 481–485.
[11]. Kroto, H.W.; Heath, J.R.; O'Brien, S.C.; Curl, R.F.; Smalley, R.E. C60: Buckminister fullerene. Nature 1985, 318,162–163.
[12]. Yang, Z.P.; Ci, L.; Bur, J.A.; Lin, S.Y.; Ajayan, P.M. Experimental observation of an extremely dark material made by a low density nano-tube array. Nano Lett. 2008, 8, 446–451.
[13]. Singer, P. CNTs an attractive alternative for interconnects (carbon nano-tubes). Semicond. Int. 2007, 30, 26–33.
[14]. Poncharal, P.; Berger, C.; Yi, Y.; Wang, Z.L.; de Heer Walt, A. Room temperature ballistic conduction in carbon nanotubes. J. Phys. Chem. 2002, 106, 12104–12118.
[15]. Iijima, S. Helical micro-tubules of graphitic carbon. Nature 1991, 354, 56–58.
[16]. Hordy, N.; Rabilloud, D.; Meunier, J.L.; Coulombe, S. High temperature and long-term stability of carbon nanotube nanofluids for direct absorption solar thermal collectors. Sol. Energy 2014, 105, 82–90.
[17]. Karami, M.; Raisee, M.; Delfani, S.; Akhavan Bahabadi, M.A.; Rashidi, A.M. Sunlight absorbing potential of carbon nanoball water and ethylene glycol-based nanofluids. Opt. Spectrosc. 2013, 115, 400–405.
[18]. Dorset, D.L.; Fryer, J.R. Quantitative electron crystallographic determinations of higher fullerenes in the hexagonal close packed polymorph. J. Phys. Chem. 2001, 105, 2356–2359.
[19]. Kuzuo, R.; Terauchi, M.; Tanaka, M.; Saito, Y.; Shinohara, H. Electron-energy-loss spectra of crystalline C 84. Phys. Rev. 1994, 49, 5054–5057.
[20]. Ge, M.; Sattler, K. Observation of fullerene cones. Chem. Phys. Lett. 1994, 220, 192–196.
[21]. Yoshitake, T.; Shimakawa, Y.; Kuroshima, S.; Kimura, H.; Ichihashi, T.; Kubo, Y.; Kasuya, D.; Takahashi, K.; Kokai, F.; Yudasaka, M.; et al. Preparation of fine platinum catalyst supported on single-wall carbon nanohorns for fuel cell application. Phys. Condens. Matter 2002, 323, 124–126.
[22]. Lee, S.Y.; Yamada, M.; Miyake, M. Synthesis of carbon nano-tubes and carbon nanofilaments over palladium supported catalysts. Sci. Technol. Adv. Mater. 2005, 6, 420–426.
[23]. Sano, N.; Akazawa, H.; Kikuchi, T.; Kanki, T. Separated synthesis of iron-included carbon nanocapsules and nanotubes by pyrolysis of ferrocene in pure hydrogen. Carbon 2003, 41, 2159–2162.
[24]. Ladjevardi, S.M.; Asnaghi, A.; Izadkhast, P.S.; Kashani, A.H. Applicability of graphite nanofluids in direct solar energy absorption. Sol. Energy 2013, 94, 327–334.
[25]. Balandin, A.A.; Ghosh, S.; Bao, W.; Calizo, I.; Teweldebrhan, D.; Miao, F.; Lau, C.N. Superior thermal conductivity of single-layer graphene. Nano Lett. 2008, 8, 902–907.
[26]. Dreyer, D.R.; Park, S.; Bielawski, C.W.; Ruoff, R.S. The chemistry of graphene oxide. Chem. Soc. Rev. 2010, 39, 228–240.
[27]. Yuan, D.; Chen, J.; Zeng, J.; Tan, S. Preparation of monodisperse carbon nanospheres for electrochemical capacitors. Electrochem. Commun. 2008, 10, 1067–1070.
[28]. Yang, R.; Qiu, X.; Zhang, H.; Li, J.; Zhu, W.; Wang, Z.; Huang, X.; Chen, L. Mono-dispersed hard carbon spherules as a catalyst support for the electro-oxidation of methanol. Carbon 2005, 43, 11–16.
[29]. Wang, Y.; Su, F.; Wood, C.D.; Lee, J.Y.; Zhao, X.S. Preparation and characterization of carbon nanospheres as anode materials in lithium-ion secondary batteries. Ind. Eng. Chem. Res. 2008, 47, 2294–2300.
[30]. Poinern, G.E.J.; Brundavanam, S.; Shah, M.; Laava, I.; Fawcett, D. Photothermal response of CVD synthesised carbon (nano) spheres/aqueous nanofluids for potential application in direct solar absorption collectors: A preliminary investigation. Nanotechnol. Sci. Appl. 2012, 5, 49–59.
[31]. Sen Gupta, S., Manoj Siva, V., Krishnan, S., Sreeprasad, T., Singh, P. K., Pradeep, T. and Das, S. K. 2011. Thermal conductivity enhancement of nanofluids containing graphene nanosheets. Journal of Applied Physics, 110: 084302-084306.

[32]. Breuer O, Sundararaj U. Big returns from small fibers: a review of polymer/carbon nanotube composites. Polym Compos 2004, 25,630-641.
[33]. Cao JX, Yan XH, Xiao Y, Ding JW. Thermal conductivity of zigzag single-walled carbon nanotubes:Role of the umklapp process. Phys Rev B 2004; 69:073407.
[34]. Fujii M, Zhang X, Xie H, Ago H, Takahashi K, Ikuta T, Abe H, Shimizu T. Measuring the thermal conductivity of a single carbon nanotube. Phys Rev Lett 2005; 95: 065502.
[35]. I. S. Awaludin, P. D. Weidman and Anuar Ishak, Stability analysis of stagnation-point flow over a stretching/shrinking sheet, AIP ADVANCES 6(4), (2016).
[36]. Maria Imtiaz, Tasawar Hayat, Ahmed Alsaedi, MHD Convective Flow of Jeffrey Fluid Due to a Curved Stretching Surface with HomogeneousHeterogeneous Reactions. Journal, Pone 11(9), (2016).
[37]. N. Sandeep, C. Sulochana, Momentum and heat transfer behaviour of Jeffrey, Maxwell and Oldroyd-B nanofluids past a stretching surface with nonuniform heat source/sink, Ain Shams Eng. Journal. (2016).
[38]. Kartini Ahmad, Zahir Hanouf, and Anuar Ishak, mixed convection Jeffrey fluid flow over an exponentially stretching sheet with magnetohydrodynamic effect, AIP ADVANCES 6, (2016)
[39]. Tasawar Hayat, Muhammad Waqas, Sabir Ali Shehzad, Ahmed Alsaedi MHD stagnation point flow of Jeffrey fluid by a radially stretching surface with viscous dissipation and Joule Heating J. Hydrol. Hydromech., 63(4) (2015).
[40]. Kalidas Das a, Nilangshu Acharya, Prabir Kumar Kundu, Radiative flow of MHD Jeffrey fluid past a stretching sheet with surface slip and melting heat transfer., Alexandria Engineering Journal 54 (2015).
[41]. Hayat T, Hussain T, Shehzad SA, Alsaedi A, Thermal and Concentration Stratifications Effects in Radiative Flow of Jeffrey Fluid over a Stretching Sheet, journal. Pone 9(10) 2014.
[42]. Sakiadis, B.C. (1961). Boundary layer behaviour on continuous solid surfaces. American Institute of Chemical Engineers Journal, 7(1), 26-28.
[43]. Crane, L.J. (1970). Flow past a stretching plate. Zeitschrift für Angewandte Mathematik und Physik, 21(4), 645–647.
[44]. Qasim, M. (2013). Heat and mass transfer in a Jeffrey fluid over a stretching sheet with heat source/sink. Alexandria Engineering Journal, 52(4), 571-575.
[45]. Cortell, R. (2014). Fluid flow and radiative nonlinear heat transfer over a stretching sheet. Journal of King Saud University-Science, 26(2), 161-167.
[46]. Ahmad, K., & Ishak, A. (2015). Magnetohydrodynamic flow and heat transfer of a Jeffrey fluid towards a stretching vertical surface. Thermal Science 2015 Online-First Issue, doi: 10.2298/TSCI141103029A.